Journal of Alloys and Compounds 789 (2019) 323–329

Contents lists available at ScienceDirect

Journal of Alloys and Compounds

journal homepage: http://www.elsevier.com/locate/jalcom

Magnetically tunable iron oxide nanotubes for multifunctional biomedical applications

Raja Das [1, 2, 3], Jason A. Cardarelli [1], Manh-Huong Phan**, Hariharan Srikanth*

Department of Physics, University of South Florida, Tampa, FL, 33620, United States

ARTICLE INFO

Article history:
Received 28 June 2018
Received in revised form
23 February 2019
Accepted 2 March 2019
Available online 5 March 2019

Keywords:
Iron oxide
Nanotubes
Magnetic hyperthermia
Biomagnetism

ABSTRACT

Design of a multifunctional magnetic bionanosystem has become increasingly important towards advancing the future of clinical medicine. While hollow iron oxide nanoparticles with enhanced surface areas allow for more drug molecules to be attached to the particles, their relatively low saturation magnetization (M_S) hinders their practicality in medicinal applications such as drug delivery and hyperthermia therapy. We demonstrate that this limitation can be overcome by utilizing 1D magnetic nanotubes that possess both enhanced surface areas and high M_S. In this study, highly crystalline, tunable aspect ratio Fe_3O_4 nanotubes have been successfully synthesized using a hydrothermal method. Magnetic measurements showed a clear Verwey transition (~120 K) and high M_S (~75 emu/g) at 300 K, confirming the high quality of the synthesized Fe_3O_4 nanotubes. Calorimetric experiments on randomly dispersed Fe_3O_4 nanotubes in water with concentration of 1 mg/mL showed a large Specific Absorption Rate (SAR) value of 400 W/g for an AC magnetic field of 800 Oe, which increased to 500 W/g when the nanotubes were aligned parallel to the DC magnetic field and suspended in a 2% agar solution. Our study shows the possibility of using the Fe_3O_4 nanotubes as a highly effective multifunctional nanoscale tool for targeted hyperthermia and on-demand drug delivery.

© 2019 Elsevier B.V. All rights reserved.

1. Introduction

The statement that cancer is the second most common cause of death in the western world is shown by the American Cancer Society's estimation that 1650 Americans died every day due to cancer complications in the year of 2017, and well over half a billion people were diagnosed with cancer in the same year [1]. Even after progress has been made to reduce cancer rates for several decades now, finding a cure and effective therapies for cancer are still included in the top priorities of international researchers [2]. Today's most commonplace treatments for cancer, though effective in many cases, can have significant downsides including surgical remedies' ineffectiveness in treating non-localized or metastasized tumors, chemotherapy's severe adverse side effects, and radiation therapy's troubles in treating metastasized cancers as well as its detrimental side effects [3–5]. With the urgency of reducing cancer casualties and the hope in finding treatments to circumvent adverse effects of common treatment options, researchers are reverently searching for improved therapies to treat cancer effectively. Nano-medicinal applications of magnetic nanoparticles (NPs) have garnered significant attention from these researchers in recent years [6,7]. Alternating current (AC) magnetic hyperthermia therapy and targeted drug delivery, the applications focused on in this work, have shown promise as such applications capable of reducing cancerous tumors [8,9].

Magnetic hyperthermia is the generation of a controlled amount of heat from magnetic nanoparticles in an AC magnetic field. There have been very promising clinical trials that prove the viability of magnetic hyperthermia for treating cancers [8]. Iron oxide NPs, particularly magnetite (Fe_3O_4) and maghemite (γ-Fe_2O_3), are the most commonly used for AC hyperthermia due to their high saturation magnetization, their biocompatibility, and their approval for medicinal applications in the United States from the Food and Drug Administration [10]. A concern with using iron oxide nanoparticles for hyperthermia therapy is the amount and concentration required for effective heat generation. With concentrations of iron oxide

* Corresponding author.
** Corresponding author.
E-mail addresses: phanm@usf.edu (M.-H. Phan), sharihar@usf.edu (H. Srikanth).
[1] Equal contribution to the work.
[2] Present address: Faculty of Materials Science and Engineering, Phenikaa Institute for Advanced Study (PIAS), Phenikaa University, Hanoi 10000, Vietnam.
[3] Phenikaa Research and Technology Institute (PRATI), A&A Green Phoenix Group, 167 Hoang Ngan, Hanoi 10000, Vietnam.

https://doi.org/10.1016/j.jallcom.2019.03.024
0925-8388/© 2019 Elsevier B.V. All rights reserved.

nanoparticles too high, the cytotoxicity of the treatment becomes so high to the point that the use of magnetic nanoparticles can damage healthy cells in the body [11–16]. Work recently conducted by our group has shown that the heating efficiency, specified as the specific absorption rate (SAR), of magnetic nanoparticles can be significantly increased through increasing the saturation magnetization (M_S) and/or the shape and magnetic anisotropy of the nanoparticles [17–20]. The anisotropy field of the nanoparticles can be increased to a value such that the heating efficiency will be optimal. But if it is too high, the nanoparticles' magnetic moments cannot follow the external AC field applied during hyperthermia experiments, resulting in reduced heating efficiency in the safe limit of the ac magnetic field amplitude that can be used for patients (This is also known as the Brezovich safe limit of the ac magnetic field amplitude and frequency being used for AC magnetic hyperthermia). By making the particles hollow the surface area available for attaching drug molecules to the particles is increased, as has been effectively shown through studies of magnetic nanoring structures designed for magnetic hyperthermia and drug delivery [21–26]. Iron oxide nanotubes are therefore ideal candidates for magnetic hyperthermia therapy and nanoparticle drug delivery. The nanotubes have the advantage of high effective anisotropy and high surface area due to their 1-dimensional and hollow morphology, respectively. Moreover, they possess high M_S value due high crystallinity of the iron oxide nanotubes.

In this paper, we report on the synthesis of highly crystallized iron oxide nanotubes using a hydrothermal method. The magnetic and hyperthermia properties of the iron oxide nanotubes are superior to those of their hollow particle counterpart, making these nanotubes desirable for multifunctional biomedical applications.

2. Synthesis and characterization of iron oxide nanotubes

First, α-Fe_2O_3 nanotubes were synthesized by a hydrothermal reaction reported previously by Jai et al. [27] In a typical reaction, an aqueous solution of $FeCl_3 \cdot 6H_2O$, $NaH_2PO_4 \cdot 2H_2O$, and Na_2SO_4 is mixed and is stirred for 30 min at room temperature. The solution was then transferred into a Teflon-lined stainless steel autoclave and heated to 220 °C. The reaction was maintained at this temperature for desired variable time. After allowing the sample to cool to room temperature, the precipitate was washed using water and ethanol.

Scanning electron microscope (SEM) images of the synthesized particles (Fig. 1) reveal that the as-synthesized nanotubes have a uniform size and shape. The nanotubes obtained after 5 h of hydrothermal reaction are with length of 460 ± 20 nm, outer diameter of 200 ± 30 nm, and wall thickness of 30 ± 2 nm. Different sizes of the nanotubes were prepared by varying the time of the hydrothermal treatment. The evolution in size of the particles based on the hydrothermal reaction time can be seen from the SEM images of the product obtained after 5 h (Sample 3), 8 h (Sample 4), 12 h (Sample 5), and 24 h (Sample 6) hours of the hydrothermal reaction (Fig. 1).

The length, outer wall diameter, and wall thickness of each sample is summarized in Table 1. The purity and the phase of the as-synthesized nanotubes were examined using X-ray diffraction (XRD). The XRD diffraction patterns of the as-synthesized nanotubes were found to closely match the indexed trigonal α-Fe_2O_3 diffraction pattern (Fig. 2).

Table 1
Size properties of nanotubes corresponding to the amount of time allowed in hydrothermal reaction. Sample 1 corresponds to 1 h of hydrothermal reaction, Sample 2–3 h, Sample 3–5 h, Sample 4–8 h, Sample 5–12 h, and Sample 6–24 h *1 h reaction yielded nanorods rather than nanotubes.

Sample	Particle Length	Outer Diameter	Wall Thickness
Sample 1	70 ± 20 nm	-*	7 ± 3 nm
Sample 2	420 ± 20 nm	160 ± 20 nm	25 ± 2 nm
Sample 3	460 ± 20 nm	200 ± 30 nm	30 ± 2 nm
Sample 4	470 ± 10 nm	170 ± 10 nm	55 ± 5 nm
Sample 5	450 ± 10 nm	200 ± 10 nm	70 ± 5 nm
Sample 6	250 ± 30 nm	160 ± 30 nm	85 ± 10 nm

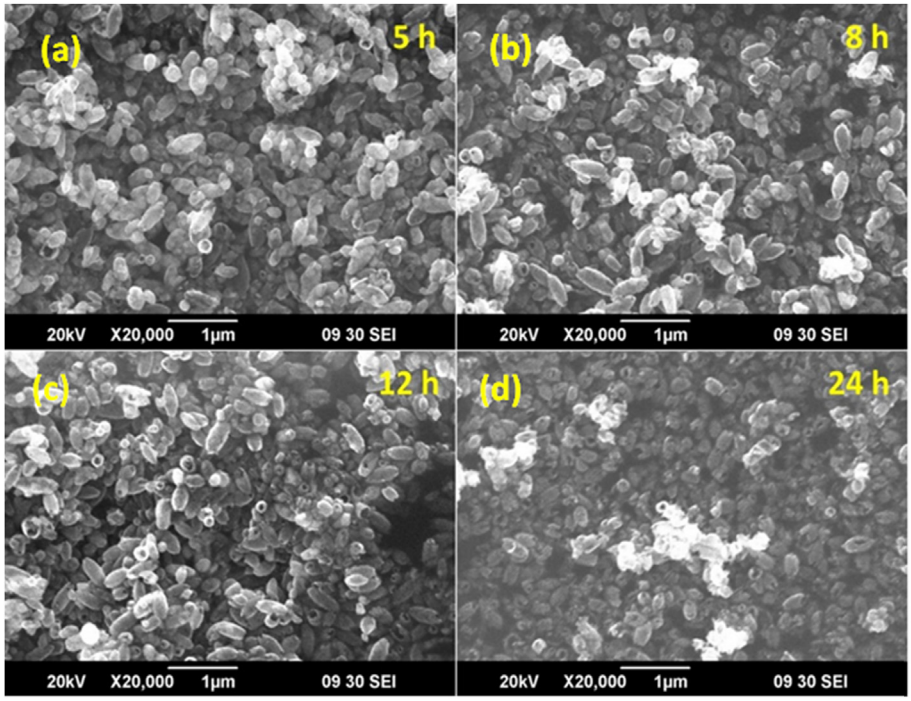

Fig. 1. SEM images of as-synthesized α-Fe_2O_3 nanotubes after hydrothermal synthesis of (a) 5-h, (b) 8-h, (c) 12-h, and (d) 24-h.

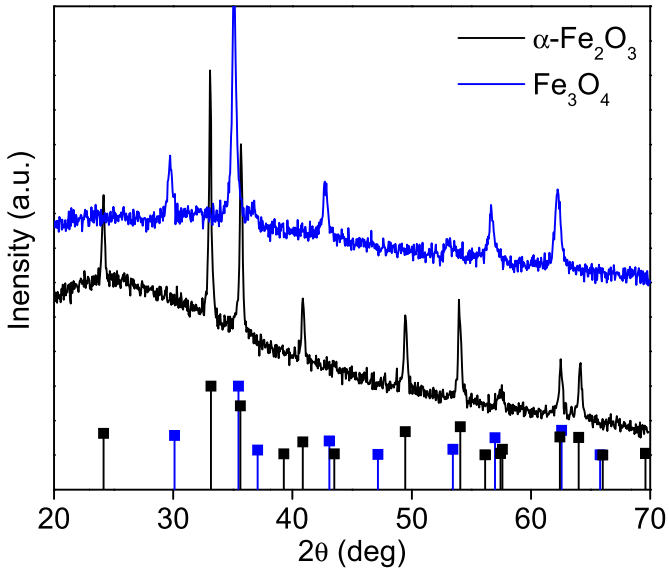

Fig. 2. X-ray diffraction (XRD) pattern of as-synthesized (α-Fe_2O_3) and calcined (Fe_3O_4) nanotubes after 8 h of reaction. The lower pattern in black and blue are for bulk α-Fe_2O_3 and Fe_3O_4 from the JCPDS data, respectively. (For interpretation of the references to colour in this figure legend, the reader is referred to the Web version of this article.)

The phase transformation of the as-synthesized α-Fe_2O_3 nanotubes into Fe_3O_4 was completed via reduction of the α-Fe_2O_3 nanotubes in presence of hydrogen/argon (7% hydrogen) [27]. The XRD pattern of the reduced nanotubes, as shown in Fig. 2, reveals the formation of single phase cubic Fe_3O_4. The reduction of α-Fe_2O_3 nanotubes to Fe_3O_4 nanotubes was done at a temperature within the range 300–360 °C for 5 h. Analysis of the resulting nanotubes revealed that when the as-synthesized nanotubes are reduced at 360 °C for 5 h, the product obtained is mixture of Fe_3O_4 and Fe_3C. When the annealing temperature was reduced to 300 °C for 5 h, pure single phase Fe_3O_4 was obtained. Thus, in order to isolate Fe_3O_4 for hyperthermia and magnetization comparisons, all of the as-synthesized nanotubes were annealed at 300 °C for 5 h for further studies. For more insight of the nanotube morphology, TEM imaging of the annealed samples were performed (Fig. 3).

TEM images of the annealed nanotubes obtained after 5 h of hydrothermal reaction showed that the nanotubes are a self-assembled structure of smaller nanorods like units which bound together to form the resulting nanotubes (Fig. 3).

To understand the possible origin on the microstructure of nanotubes, we investigated the growth process by studying the time dependent morphology evolution (Fig. 3). The as-synthesized particles obtained after 1 h (Sample 1) of reaction shows the formation of 70 ± 20 nm long and 7 ± 3 nm width nanorods. Extending the reaction to 3 h (Sample 2) yielded nanotubes with outer-diameter of 160 ± 20 nm, wall thickness of 25 ± 2 nm and length of 420 ± 20 nm. With further prolonging the reaction the length and outer diameter of the nanotubes remain almost constant but the wall thickness increase with reaction time. From the SEM image (Fig. 1) of the 24-h sample it was found that the length and outer diameter of the nanotubes are decreased compared to 12 h sample. From TEM image of the reduced Fe_3O_4, it can be seen that the nanotubes are broken and degraded in 24 h sample (Fig. 3). This could be due to the breaking of the individual nanotubes to its constituent nanorod-like structures which assembled to form the nanotubes.

It was found that the nanorods obtained after the breakdown of the 24 h samples has the same dimension as the 1 h reaction sample. This further suggests that the nanotubes are made up of constituent self-assembled nanorods. It should be noted that the morphology difference between the 24 h nanotubes before and after reduction could be due temperature induced breaking of the α-Fe_2O_3 nanotubes. Some of the as-synthesized α-Fe_2O_3 nanotubes had begun breaking during hydrothermal treatment and the final breakdown happens during reduction process. Schematic of morphology and crystal structure evolution of the α-Fe_2O_3 nanotubes with reaction time and calcination is shown in Fig. 4.

Magnetic measurements of the Fe_3O_4 nanotubes confirm the high saturation magnetization (M_S), as can be seen in Fig. 5a. The coercive field (H_C) at 300 K and the M_S values of the Fe_3O_4

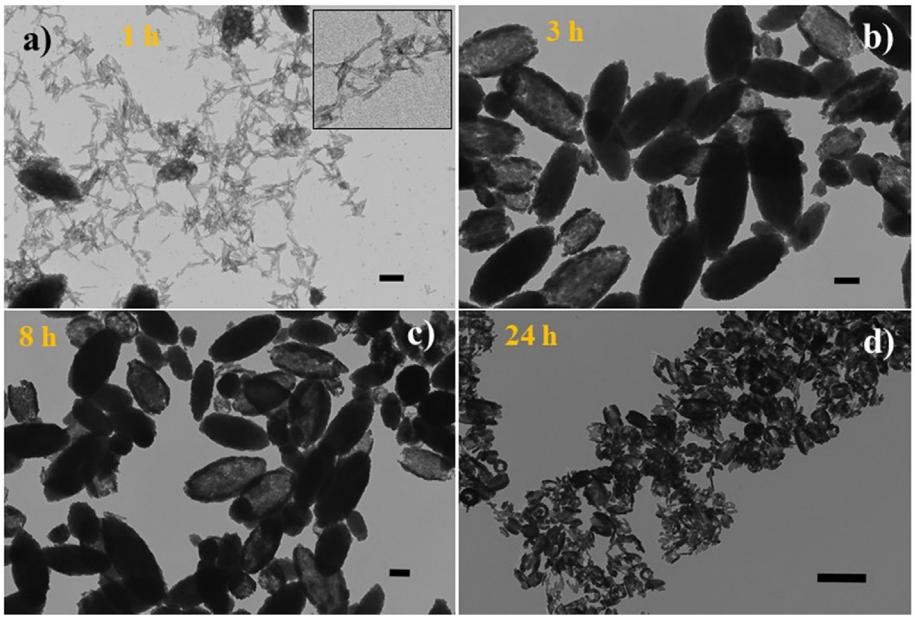

Fig. 3. Transmission electron microscope (TEM) images of Fe_3O_4 nanotubes after different reaction time a) 1 h, b) 3 h, c) 8 h, d) 24 h. Scale bars a-c) 100 nm, d) 500 nm. Inset of a) shows the zoom view of the nanorods formed after 1 h of reaction.

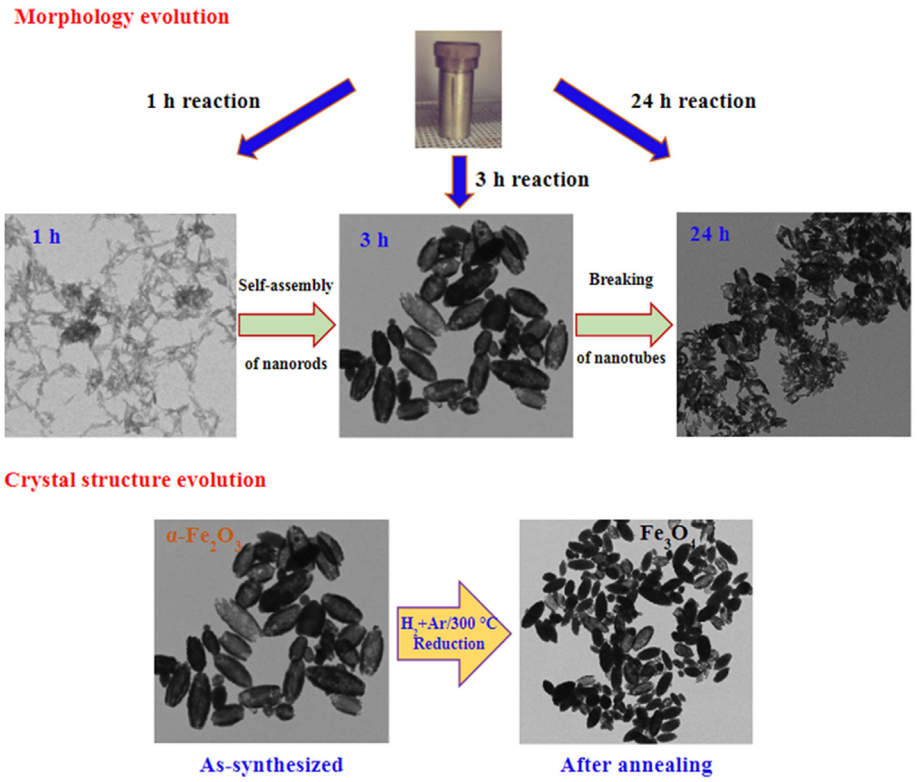

Fig. 4. Schematic of morphology and crystal structure evolution of the Fe_3O_4 nanotubes with reaction time and calcination.

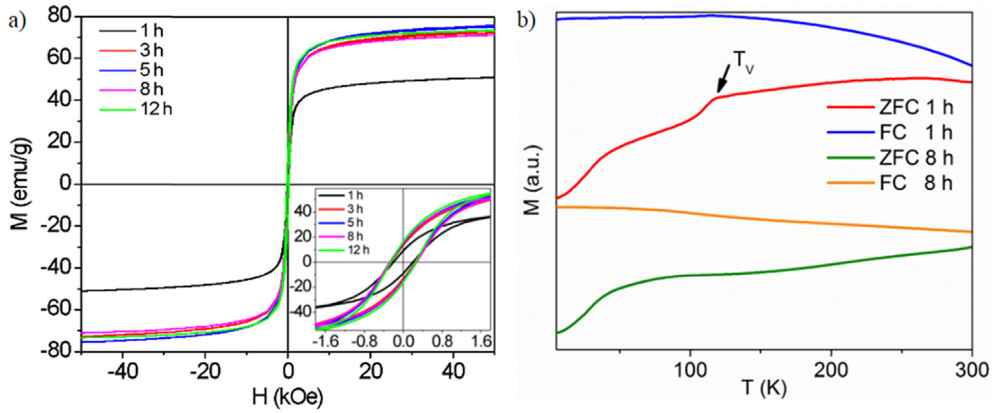

Fig. 5. Magnetic characterization of Fe_3O_4 nanotubes: a) Room temperature M – H loops, b) temperature dependent zero-field cooled (ZFC) and field-cooled (FC) magnetization curves for various Fe_3O_4 nanotubes measured at 100 Oe.

nanotubes of different hydrothermal sample times can be seen in Table 2. The H_C values for all the nanotubes samples are almost same (Table 2). There is very small variation of the H_C values with increase in reaction time. It can be seen in this table that the largest value of M_S (~75 emu/g) is achieved for Sample 3, among the samples investigated. This value is smaller than those of bulk Fe_3O_4 (M_S ~87 emu/g) and the Fe_3O_4 nanorods [12] (M_S ~87 emu/g), but is much greater than that of Fe_3O_4 hollow nanoparticles (M_S ~40 emu/g) [28]. The smaller M_S of the nanotubes as compared to the nanorods [12] could be due to the larger surface to volume ratio and the lower crystalline quality of the nanotubes. The larger value of M_S for the nanotubes is shown to yield a higher heating efficiency (a larger SAR value) as compared to its hollow NP counterpart. It should also be noticed in Table 2 and Fig. 5a that all nanotube samples exhibit non-zero coercive fields (H_C) and remnant magnetization (Mr) at room temperature, indicating that they are typically soft ferromagnets rather than superparamagnetic materials. The temperature dependence of the field cooled and zero-

Table 2
Magnetic parameters of the nanotube samples after undergoing hydrogen/argon reduction: saturation magnetization (M_S), coercive field (H_C), remnant magnetization (M_r), and M_r/M_S ratio at temperature of 300 K of samples 1–5.

Samples	M_S	H_C	M_r	M_r/M_S
Sample 1	51 emu/g	196 Oe	9.0 emu/g	0.176
Sample 2	72 emu/g	243 Oe	13.5 emu/g	0.188
Sample 3	75 emu/g	252 Oe	14.7 emu/g	0.196
Sample 4	71 emu/g	273 Oe	15.3 emu/g	0.215
Sample 5	74 emu/g	252 Oe	16.1 emu/g	0.218

field cooled (ZFC) magnetization was performed to further determine the low temperature magnetic behavior of the nanotubes (Fig. 5b).

For both Sample 1 and Sample 4, ZFC magnetization curves showed a transition near 120 K, which can be assigned to the metal-insulator transition associated with the crystal structure of Fe_3O_4. It is often true of nanoparticles that the Verwey transition is suppressed due to poor crystallinity and defects [13]. The presence of the Verwey transition in nanostructures indicates the formation of high-quality and pure phase Fe_3O_4 nanostructures, and this is true for the case of our Fe_3O_4 nanotube samples [29–31].

In order to evaluate the magnetic hyperthermia performance of these nanotubes, the SAR values were calculated by using calorimetric measurements. It is worth mentioning that when the particles size is larger (typically more than 100 nm), the particles are removed only by the phagocytosis whereas smaller particles are removed by all types of cells by pinocytosis. Under biological conditions, particles larger than 10 nm cannot penetrate the endothelium. However, this permeability barrier may be increased under pathologic conditions, such as inflammation or tumor infiltration. Under these conditions, the penetration threshold can be increased to allow 700 nm particles. This can also be temporarily achieved through the help of medication, immune modulators, heat or radiation. Therefore, the nanotubes presented in this study can be used in both magnetic hyperthermia and drug delivery. However before using these nanotubes for magnetic hyperthermia and drug delivery applications, surface functionalization and cytotoxicity studies are needed.[32] The heating efficiency measurements of the nanotubes were performed with a particles concentration of 1 mg/ml in both water and agar (both randomly oriented and DC-magnetic field aligned). Fig. 6a represents the SAR vs field when the samples were dispersed in water with a concentration of 1 mg/ml. As can be observed at 200 Oe applied field the SAR (heating efficiency) of all the samples were very small. This could be due to the fact that the coercive field of the samples being close to or above 200 Oe. It should be highlighted that the coercive field of the samples at 300 K are in the range of 250 Oe for the nanotubes (Samples 2–5) and 200 Oe for the Sample 1 nanorods.

As the field is increased above the coercive field of the nanotubes, the SAR values showed an improvement and this improves further with increase in applied field. It can be seen that the heating efficiencies of the nanotubes are almost same for all the samples. This could be due to similar saturation magnetization and coercive field values of the nanotubes. The SAR value for Sample 1 is smaller than other nanotubes (3–12 h) at all the measured fields. This is due to the smaller values of M_S and H_C of Sample 1 compared with the other nanotubes. Randomly dispersed Fe_3O_4 nanotubes in water (1 mg/ml) showed a large SAR value of 345 W/g (Sample 2) and 360 W/g (Sample 5) for an AC magnetic field of 800 Oe. In order to separate the Néel and Brownian contribution of SAR, measurements were performed by embedding the particles in 2% weight agar. The high viscosity of the agar restricts the physical motion of the particles, and moreover agar effectively simulates the cell environment which is important for the nanotubes' real in vivo application. The results showed that the heating efficiency of the samples remain almost same in both water and agar (random) till applied magnetic field of 400 Oe (Fig. 6b). At 600 and 800 Oe the heating efficiency of the randomly dispersed samples suspended in agar reduces by 20% compared to the water dispersed sample. This indicated that at field values higher than 400 Oe there is an about 20% contribution of either Brownian motion of nanotubes towards the heating efficiency when suspended in water or due to the difference in motion and alignment efficiency of particles in water vs agar. This contribution is first significantly noticed in our

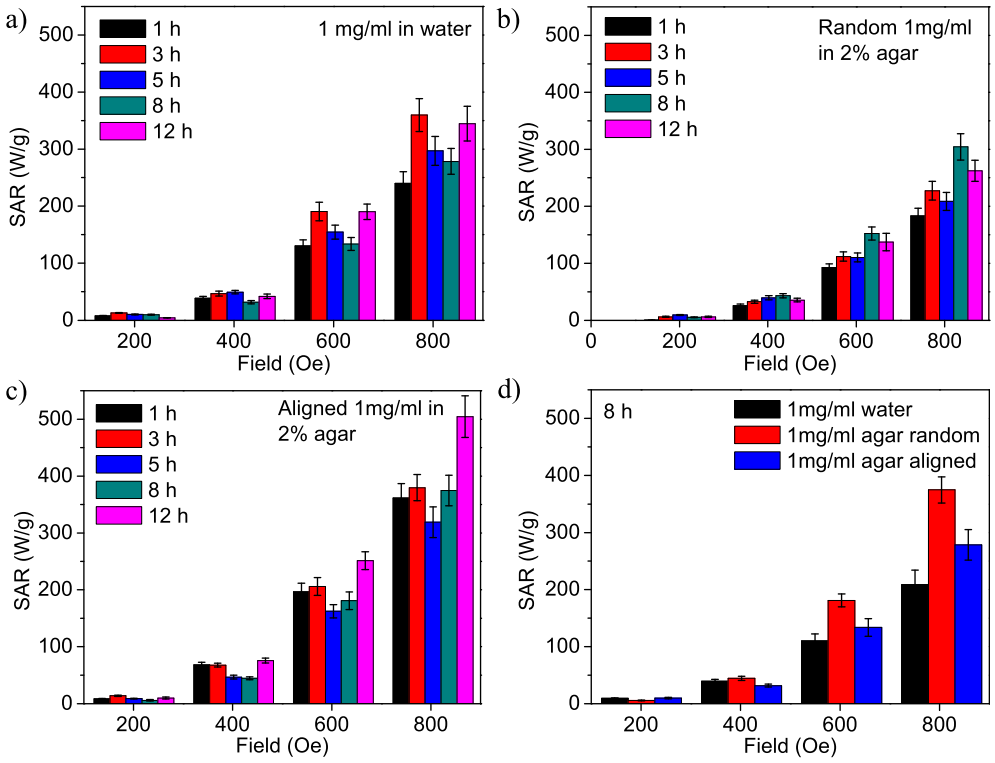

Fig. 6. Specific Absorption Rate (SAR) measurements for all of the nanotube samples with the conditions of (a) the particles suspended in water, (b) the particles randomly suspended in 2% agar solution, (c) the particles aligned to an external magnetic field suspended in 2% agar solution. The water, agar and agar aligned samples are compared using the (d) 8-h nanotubes.

measurements at field strengths of 600 Oe and higher for most nanotube samples, and at 400 Oe and higher for the 1 h nanorod samples. In our previous study on Fe_3O_4 nanorods, we observed a large increase in heating efficiency of the nanorods when they were aligned in the field direction compared to randomly oriented samples.

To study the effect of alignment of the nanotubes on the heating efficiency, the samples were aligned in a uniform direction in agar solution using a DC magnetic field produced by a permanent magnet. It is found that the heating efficiency of all the samples improved in aligned samples compared to the randomly dispersed ones (Fig. 6c).

It is worth noting that the heating efficiency of the aligned samples did not improve when the applied field is 200 Oe. This shows that when the applied field is below the particles' effective anisotropic field, the alignment of the sample does not have any effect on the heating efficiency. As all the samples showed similar values of SAR, we choose 8 h samples for the detailed study. It can be seen that at an applied AC field of 200 Oe the SAR value remains almost constant in water, and agar (random and aligned). This could be due to the fact that 200 Oe is below the coercive field of the sample so applied field does not have any influence on the SAR value. At an applied field of 400 Oe and above there is a decrease in SAR value in the randomly aligned sample as compared to water and this increases with increase in applied AC magnetic field. A maximum decrease in SAR in the randomly aligned sample as compared to water was seen at 800 Oe applied AC field where SAR decreased from 279 W/g in water to 205 W/g in randomly aligned in agar (Fig. 6d). As the strength of the AC magnetic field is increased the obtained SAR values are almost similar till an applied field of 400 Oe in both water and agar (aligned and randomly aligned). A 65%, 80% improvement in SAR was observed in the aligned sample at an applied field of 600 and 800 Oe, respectively. This improvement in SAR values in the aligned sample compared to the randomly aligned sample demonstrated that SAR of the anisotropic nanostructures may be improved when the field is applied parallel to the particles alignment direction. Finally, it is worth mentioning that while the Fe_3O_4 hollow nanoparticles possess a limited value of SAR (~6 W/g at an ac field of 800 Oe) [28], a much greater value of SAR (~350 W/g) is achieved for our Fe_3O_4 nanotubes. This is because the M_S of the Fe_3O_4 hollow nanoparticles (M_S ~18 emu/g) is about 4 times smaller than that of the Fe_3O_4 nanotubes (M_S ~75 emu/g). These results indicate the superior advantage of the Fe_3O_4 nanotubes being ideal for dual-purpose applications in localized magnetic hyperthermia and targeted drug delivery.

3. Conclusions

In conclusion, highly-crystalline, hollow Fe_3O_4 nanotubes have been synthesized by two-step synthesis involving a reduction of hydrothermally-synthesized α-Fe_2O_3 nanotubes. Systematic study of the growth mechanism of the nanotubes indicates that the nanotubes are made up of self-assembled composite nanorods. The growth mechanism was tracked using SEM and TEM microscopy techniques and comparing images taken of as-synthesized particles removed from the hydrothermal synthesis reaction at varied durations of reaction time. Measurements of the magnetization of the synthesized Fe_3O_4 nanotubes confirm the high crystalline quality and saturation magnetization of the subject nanotubes of this study. These measurements show a clear Verwey transition, indicating the high uniformity of the particles' magnetite composition and phase. Chemical composition and crystalline phase of the particles were confirmed using X-ray diffraction techniques. Calorimetric experiments of Fe_3O_4 nanotubes showed a large SAR value, which is much greater than that of their hollow counterparts and increases 80% when the nanotubes were aligned parallel to the DC magnetic field. Our study shows the strong potential of using the Fe_3O_4 nanotubes as an ideal vehicle for dual-purpose applications in hyperthermia and on-demand drug delivery.

Acknowledgments

Research at the University of South Florida was supported by the U.S. Department of Energy, Office of Basic Energy Sciences, Division of Materials Sciences and Engineering under Award No. DE-FG02-07ER46438.

References

[1] American Cancer Society, Cancer Facts and Figures 2017, American Cancer Society, Atlanta, 2017.
[2] S. Simon, Cancer Facts and Figures: Death Rate Down 25% since 1991, 2017, January 5. Retrieved from cancer.org, https://www.cancer.org/latest-news/cancer-facts-and-figures-death-rate-down-25-since-1991.html.
[3] American Cancer Society, Cancer Surgery, 2016, April 12. Retrieved from cancer.org, https://www.cancer.org/treatment/treatments-and-side-effects/treatment-types/surgery/how-surgery-is-used-for-cancer.html.
[4] Cancer Research UK, 2017, November 17. Retrieved from, cancerresearchuk.org, http://www.cancerresearchuk.org/about-cancer/cancer-in-general/treatment/chemotherapy/side-effects/about.
[5] National Cancer Institute, Radiation Therapy for Cancer, 2010, June 30. Retrieved from cancer.org, https://www.cancer.gov/about-cancer/treatment/types/radiation-therapy/radiation-fact-sheet.
[6] G. Glockl, R. Hergt, M. Zeisberger, S. Dutz, S. Nagel, W. Weitschies, The effect of field parameters, nanoparticle properties and immobilization on the specific heating power in magnetic particle hyperthermia, J. Phys. Condens. Matter 18 (28) (2006) 2935.
[7] B. Thiesen, A. Jordan, Clinical applications of magnetic nanoparticles for hyperthermia, Int. J. Hyperth. 24 (6) (2008) 467–474.
[8] A. Ito, M. Shinkai, H. Honda, T. Kobayashi, Medical application of functionalized magnetic nanoparticles, J. Biosci. Bioeng. 100 (1) (2005) 1–11.
[9] A. Jordan, R. Scholz, P. Wust, H. Fahling, R. Felix, Magnetic fluid hyperthermia (MFH): cancer treatment with AC magnetic field induced excitation of biocompatible superparamagnetic nanoparticles, J. Magn. Magn. Mater. 201 (1–3) (1999) 413–419.
[10] M. Mahmoudi, A. Simchi, M. Imani, Recent advances in surface engineering of superparamagnetic iron oxide, J. Iran. Chem. Soc. 7 (2010) S1–S27.
[11] R. Hergt, S. Dutz, Magnetic particle hyperthermia—biophysical limitations of a visionary tumour therapy, J. Magn. Magn. Mater. (2007) 187–192.
[12] C.C. Berry, S. Wells, S. Charles, G. Aitchison, A.S.G. Curtis, Cell response to dextran-derivatised iron oxide nanoparticles post internalization, Biomaterials 25 (2004) 5405–5413.
[13] I. Hilgera, S. Fruhauf, W. Linb, R. Hiergeistc, W. Andra, R. Hergtc, W.A. Kaiser, Cytotoxicity of selected magnetic fluids on human adenocarcinoma cells, J. Magn. Magn. Mater. 261 (2003) 7–12.
[14] S. Naqvi, M. Samim, M.Z. Abdin, F.J. Ahmed, A.N. Maitra, C.K. Prashant, A.K. Dinda, Concentration-dependent toxicity of iron oxide nanoparticles mediated by increased oxidative stress, Int. J. Nanomed. 5 (2010) 983–989.
[15] Z.G.M. Lacava, R.B. Azevedo, E.V. Martins, L.M. Lacava, M.L.L. Freitas, V.A.P. Garcia, C.A. Rebula, A.P.C. Lemos, M.H. Sousa, F.A. Tourinho, M.F. Da Silva, P.C. Morais, Biological effects of magnetic fluids: toxicity studies, J. Magn. Magn. Mater. 201 (1999) 431–434.
[16] Y. Zhang, N. Kohler, M. Zhang, Surface modification of superparamagnetic magnetite nanoparticles and their intracellular uptake, Biomaterials 23 (2002) 1553–1561.
[17] R. Das, J. Alonso, Z. Porshokouh, V. Kalappattil, D. Torres, M.-H. Phan, E. Garaio, J.A. Garcia, J.L.S. Liamazares, H. Srikanth, Tunable high aspect ratio iron oxide nanorods for enhanced hyperthermia, J. Phys. Chem. C 120 (18) (2016) 10086–10093.
[18] Z. Nemati, J. Alonso, I. Rodrigo, R. Das, E. Garaio, J.A. Garcia, I. Orue, M.H. Phan, H. Srikanth, Improving the heating efficiency of iron oxide nanoparticles by tuning their shape and size, J. Phys. Chem. C (2018) 2367–2381.
[19] Z. Porshokouh, S.M. Salili, J. Masa, A. Ataie, R. Das, M. Phan, H. Srikanth, Superparamagnetic iron oxide nanodiscs for hyperthermia therapy: does size matter? J. Alloys Compd. (2017) 709–714.
[20] R. Das, N. Rinaldi-Montes, J. Alonso, Z. Amghouz, P. Gorria, J.A. Blanco, M.H. Phan, H. Srikanth, Boosted hyperthermia therapy by combined AC magnetic and photothermal exposures in Ag/Fe3O4 nanoflowers, ACS Appl. Mater. Interfaces (2016) 25162–25169.
[21] K. Cheng, S. Peng, C. Xu, S. Sun, Porous hollow Fe_3O_4 nanoparticles for targeted delivery and controlled release of cisplatin, J. Am. Chem. Soc. (2009) 10637–10644.
[22] J. Shin, R.M. Anisur, M.K. Ko, G.H. Im, J.H. Lee, I.S. Lee, Hollow manganese oxide nanoparticles as multifunctional agents for magnetic resonance imaging and

drug delivery, Angew. Chem. Int. Ed. (2008) 321–324.
[23] X. Huang, X. Meng, F. Tang, L. Li, D. Chen, H. Liu, J. Ren, Mesoporous magnetic hollow nanoparticles-protein carriers for lysosome escaping and cytosolic delivery, Nanotechnology (2008) 445101.
[24] R. Xing, A.A. Bhirde, S. Wang, X. Sun, G. Liu, Y. Hou, X. Chen, Hollow iron oxide nanoparticles as multidrug resistant drug delivery and imaging vehicles 6 (1) (2013) 1–9.
[25] C.S.B. Dias, T.D.M. Hanchuk, H. Wender, W.T. Shigeyosi, J. Kobarg, A.L. Rossi, M.N. Tanaka, M.B. Cardoso, F. Garcia, Shape tailored magnetic nanorings for intracellular hyperthermia cancer therapy, Sci. Rep. 7 (2017) 14843.
[26] X.L. Liu, Y. Yang, C.T. Ng, L.Y. Zhao, Y. Zhang, B.H. Bay, H.M. Fan, J. Ding, Magnetic vortex nanorings: a new class of hyperthermia agent for highly efficient in vivo regression of tumors, Adv. Mater. 27 (2015) 1939–1944.
[27] C.J. Jia, L.D. Sun, F. Luo, X.D. Han, L.J. Heyderman, Z.-G. Yan, C.H. Yan, K. Zheng, Z. Zhang, M. Takano, N. Hayashi, M. Eltschka, M. Kläui, U. Rüdiger, T. Kasama, L.C. Gontard, R.E.D. Borkowski, G. Tzvetkov, J. Raabe, Large-scale synthesis of single-crystalline iron oxide magnetic nanorings, J. Am. Chem. Soc. 130 (50) (2008) 16968–16977.
[28] Z. Nemati, J. Alonso, H. Khurshid, M.H. Phana, H. Srikanth, Core/shell iron/iron oxide nanoparticles: are they promising for magnetic hyperthermia? R. Soc. Chem. Adv. (2016) 38697–38702.
[29] F. Walz, The Verwey transition - a topical review, J. Phys. Condens. Matter (2002) R285.
[30] E.J. Verwey, Electronic conduction of magnetite (Fe_3O_4) and its transition point at low temperatures, Nature (1939) 327–328.
[31] P. Poddar, T. Fried, G. Markovich, First-order metal-insulator transition and spin-polarized tunneling in Fe_3O_4 nanocrystals, Phys. Rev. B 65 (2002) 172405.